Available online at www.sciencedirect.com
SCIENCE DIRECT®
Journal of Solid State Chemistry 170 (2003) 211–220
JOURNAL OF SOLID STATE CHEMISTRY
http://elsevier.com/locate/jssc

Oxygen/fluorine ordering, structured diffuse scattering and the local crystal chemistry of $K_3MoO_3F_3$

R.L. Withers,* T.R. Welberry, F.J. Brink,[1] and L. Norén

Research School of Chemistry, Australian National University, GPO Box 4, Canberra, ACT 0200, Australia

Abstract

Bond valence sum calculations are used to investigate the crystal chemistry of the elpasolite-related oxyfluoride $K_3MoO_3F_3$ in order to obtain insight into the type/s of structural distortion (away from an ideal, high symmetry, elpasolite type parent structure) responsible for a characteristic, highly structured, three-dimensional diffuse intensity distribution. The first required type of local structural distortion corresponds to large amplitude MoO_3F_3 octahedral rotations while the second is associated with O/F ordering and associated induced Mo ion shifts. Monte Carlo modelling is used to show how the latter when coupled with an appropriate local crystal chemical constraint can give rise to the observed structured diffuse scattering. The study is part of a wider search for diffraction evidence of oxygen/fluorine ordering in metal oxyfluoride systems.

1. Introduction

$K_3MoO_3F_3$ is one member of a rather large group of oxyfluoride phases ($A_2^{1+}B^{1+}M^{IV}OF_5$ (A, B = an alkali ion; M^{IV} = Ti, V), $A_2^{1+}B^{1+}M^{V}O_2F_4$ (A, B = alkali; M^{V} = V, Nb) and $A_2^{1+}B^{1+}M^{VI}O_3F_3$ (A, B = K, Rb, Cs; M^{VI} = Mo, W)) [1–2] which are reported to crystallize either in the ideal cubic ($Fm\bar{3}m$) A_2BMX_6 elpasolite (ordered perovskite) structure type (see Fig. 1) or in closely related modulated variants thereof [1–4]. They are of interest as a result of their intriguing ferroelectric and ferroelastic phase transition behavior as well as the question of O/F ordering therein. $K_3MoO_3F_3$ itself undergoes two reversible structural phase transitions on cooling from above 522 K. The first is from the cubic ($Fm\bar{3}m$) γ polymorph of supposedly ideal elpasolite structure type (above 522 K) through an intermediate (ferroelectric and also reported to be ferroelastic) β polymorph (436 K $< T <$ 522 K) to a lowest temperature (ferroelectric as well as ferroelastic) α polymorph (below 436 K) [5–7]. While the optical and dielectric properties of these materials have been intensively studied [5–7], the corresponding crystallographic properties are far less well understood.

Like many other oxyfluoride systems [8], random anion site disorder has invariably been reported for the anion, or X, site positions of these phases [1,9] despite the two chemically quite distinct anion species and evidence from bond valence sum calculations [10] suggesting that there ought to be quite a strong driving force for local crystal chemical ordering and associated structural distortion (see below and Ref. [11]). The similarity in scattering power of oxygen and fluorine for any of the common diffraction techniques [12,13] considerably complicates the search for direct evidence of O/F ordering. Bond valence sum calculations can be used to distinguish O occupied sites from F occupied sites when O/F ordering is complete and no disorder occurs [13,14]. Where true long range O/F ordering does not exist, however, it is necessary to look for more subtle diffraction features such as structured diffuse scattering, typically a consequence of the correlated displacive relaxation of the cations induced by local O/F ordering [15,16].

Highly structured diffuse scattering of this general type has recently been identified and interpreted in terms of specific patterns of O/F ordering for two particular oxyfluoride systems, FeOF of rutile type structure [15] and NbO_2F of perovskite type structure [16]. In the case of FeOF, the observed diffuse distribution took the (relatively simple) form of one-dimensional rods of

*Corresponding author. Fax: 26-12-507-50.
E-mail address: withers@rsc.anu.edu.au (R.L. Withers).
[1] Also at Electron Microscope Unit, Research School of Biological Sciences, Australian National University, Canberra, ACT 0200, Australia.

0022-4596/03/$ - see front matter © 2002 Elsevier Science (USA). All rights reserved.
doi:10.1016/S0022-4596(02)00036-1

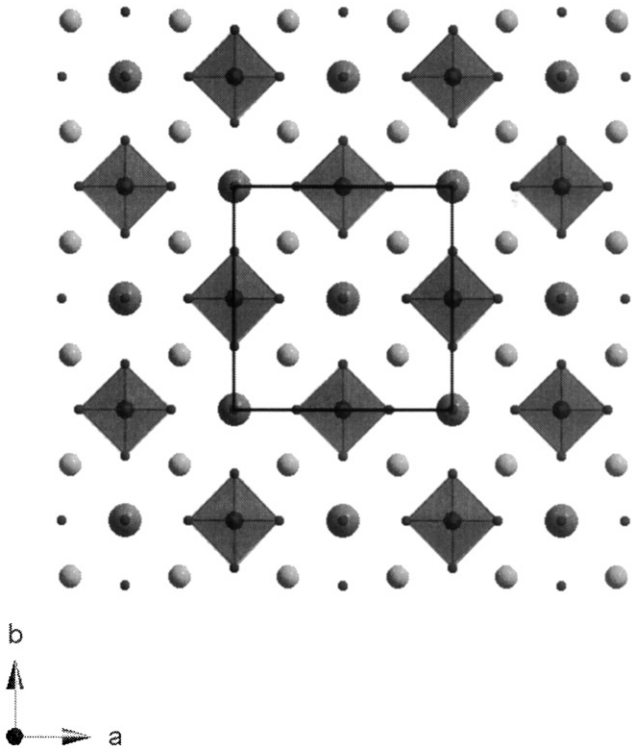

Fig. 1. Schematic {001} section (from $z = 0.2$ to 0.8) of the ideal cubic $Fm\bar{3}m$ $K(1)_2K(2)MoX_6$ (X =O, F) elpasolite parent structure type. The MoX_6 octahedra in this section are denoted by the gray octahedra and the anions by the smallest dark balls. The K(1) cations are represented by the smaller gray balls while the K(2) cations are represented by the largest darker balls. An equivalent such section but translated by $\frac{1}{2}(\mathbf{b}+\mathbf{c})$ occurs above and below each such section. Note that each K(2) cation is thus surrounded by an octahedra of MoX_6 octahedra.

diffuse intensity implying two-dimensional (planar) O/F ordering and associated induced Fe shifts (within local FeO_3F_3 octahedra) [15]. In the case of NbO_2F, two co-existing but quite distinct types of diffuse distribution were observed. The first type of observed diffuse distribution, and the one associated with local O/F ordering, took the (again relatively simple) form of two-dimensional sheets of diffuse intensity implying one-dimensional (columnar) O/F ordering and associated induced structural relaxation [16]. A second quite distinct type of diffuse distribution in the form of $\langle\frac{1}{2},\frac{1}{2},\zeta rangle*$ rods of diffuse intensity was also observed. This second type of diffuse distribution was shown to arise from correlated octahedral rotation modes. Both types of structural distortion were shown to be necessary to satisfy local crystal chemical requirements [16].

In the case of $K_3MoO_3F_3$, instead of the above relatively simple forms of diffuse distributions, a recent electron diffraction study [11] reported the existence of a complex, three-dimensional, continuous diffuse intensity distribution, presumably also arising from O/F ordering and/or associated structural distortions acting to improve local crystal chemistry. The interpretation of such a complex diffuse distribution, however, was by no means immediately apparent. In the room temperature α polymorph, this complex diffuse distribution was shown to co-exist with sharp, although weak, satellite reflections characteristic of a monoclinic, long period superstructure phase ($I1a1$, $\mathbf{a} = 2\mathbf{a}_p - \mathbf{c}_p, \mathbf{b} = 4\mathbf{b}_p, \mathbf{c} = \mathbf{a}_p + 2\mathbf{c}_p$ when expressed in terms of the underlying elpasolite parent structure type). Upon heating above the polymorphic α to β phase transition, the satellite reflections disappear suddenly [5] but the diffuse distribution remains [11].

It was suggested that the highly structured, characteristic diffuse intensity distribution must arise from some type of local O/F ordering constraint and associated structural relaxation [11]. At the time, however, no particular model for this local O/F ordering could even be envisaged let alone tested. The primary purpose of the current contribution is to use Monte Carlo modelling to show how O/F ordering and associated structural relaxation arising from local crystal chemical constraints can give rise to the observed structured diffuse scattering. In order to gain insight into the likely type/s of local structural distortion away from the ideal high symmetry parent structure that might be responsible for the observed diffuse distribution, bond valence sum calculations are first used to investigate the crystal chemistry of $K_3MoO_3F_3$. The study is part of a wider search for diffraction evidence of oxygen/fluorine ordering in metal oxyfluoride systems.

2. Local crystal chemical considerations

The ideal high symmetry, $Fm\bar{3}m$ elpasolite structure type (K(1) at $\frac{1}{4},\frac{1}{4},\frac{1}{4}$; K(2) at $\frac{1}{2},\frac{1}{2},\frac{1}{2}$; Mo at 0, 0, 0 and X or (O,F) at x, 0, 0—see Fig. 1) has only two structural degrees of freedom, namely the overall lattice parameter a_p and the x fractional co-ordinate of the anion position. There are, however, five constituent ions whose local crystal chemical requirements need to be satisfied. It should not therefore be surprising that the two symmetry-allowed structural degrees of freedom are insufficient to simultaneously satisfy the competing bond valence requirements of all five constituent ions of the ideal $Fm\bar{3}m$ elpasolite structure type.

Fig. 2, for example, shows a plot of the percentage deviation in calculated bond valence sum (or Apparent Valence, AV) away from the ideal AV [10], $\Delta(AV)/AV$, for each of these five constituent ions as a function of the unknown x fractional co-ordinate of the anion position. A value of 8.68 Å has been used for the overall lattice parameter a_p, appropriately given the metrically tetragonal cell dimensions for the underlying average structure of $K_3MoO_3F_3$ at room temperature of $8.66 \times 8.66 \times 8.72$ Å [11]. (The refined value of x for the high temperature phase of the closely related

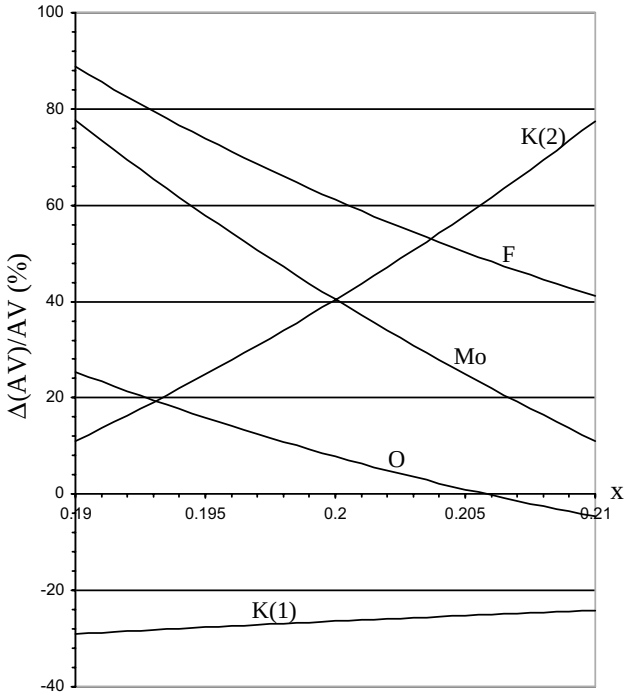

Fig. 2. Plot of $\Delta(\mathrm{AV})/\mathrm{AV}$ (expressed as a percentage) for each of the five constituent ions of $K(1)_2K(2)MoO_3F_3$ in the ideal $Fm\bar{3}m$ elpasolite structure type as a function of the unknown x fractional co-ordinate of the anion position. A value of 8.68 Å has been used for the overall lattice parameter a_p (appropriate given the metrically tetragonal cell dimensions for the underlying average structure of $K_3MoO_3F_3$ at room temperature of $8.66 \times 8.66 \times 8.72$ Å).

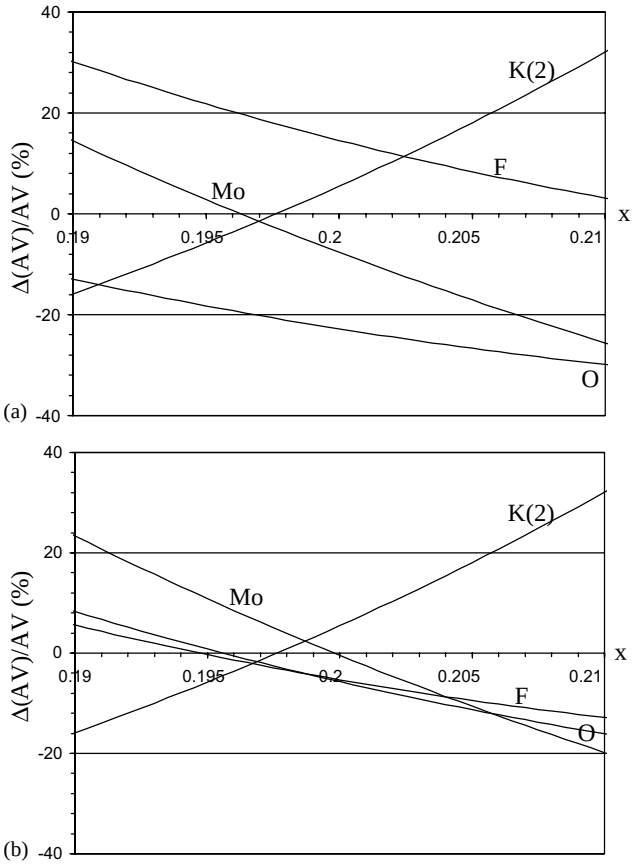

Fig. 3. Plot of $\Delta(\mathrm{AV})/\mathrm{AV}$ for K(2), Mo, O and F as a function of x after allowing (a) for a 0.75 Å transverse shift of the anion positions and (b) an additional 0.105 Å shift of the Mo ions away from the F ions and towards the O ions within each (assumed) MoO_3F_3 octahedra.

material $Rb_2KMoO_3F_3$ [9] is $x = 0.2105$). AV calculations suggest that a more likely value for x in the case of $K_3MoO_3F_3$ would be around 0.20. It is apparent from Fig. 2 that it is simply not possible to even come close to satisfying the competing bond valence requirements of all five constituent ions of $K(1)_2K(2)MoO_3F_3$ while remaining in the ideal elpasolite structure type, regardless of what value is used for x.

One or other of the Mo and K(2) ions, for example, are a minimum of 40% over-bonded (at $x \sim 0.20$) whatever value of x is used. Similarly a large, and crystal chemically undesirable, splitting in the $\Delta(\mathrm{AV})/\mathrm{AV}$ curves of O and F is also apparent, again whatever value of x is used (see Fig. 2). Clearly significant amplitude local structural distortions are going to be necessary to remedy such crystal chemical deficiencies. That there is likely to be plenty of scope for such local structural distortion is reflected, for example, in the very large amplitude thermal parameters refined for the closely related, $Fm\bar{3}m$ elpasolite type average crystal structure of $Rb_2KMoO_3F_3$ [9]. (The equivalent average structure refinement for $K_3MoO_3F_3$ has yet to be carried out.)

A clue as to one type of structural distortion that must be occurring on the local scale can be obtained from the refined "significantly anisotropic" thermal vibrations of the anions in the closely related, elpasolite type average crystal structure of $Rb_2KMoO_3F_3$ [9]. Values for u_{11} of 0.148 and u_{22} of 0.257 at 343 K, for example, imply significant ($\sim$0.5–0.6 Å) transverse displacements of the anions perpendicular to the local Mo–X–K(2) directions (see Fig. 1). In the case of $K_3MoO_3F_3$, AV calculations (cf. Fig. 2 with Fig. 3) suggest the magnitude of such transverse anion shifts will need to be even larger ($\sim$0.7–0.8 Å) in order to sufficiently reduce the significant over-bonding of the K(2) and Mo ions (Fig. 3(a) has been calculated assuming 0.75 Å transverse shifts of the anions). Such large amplitude, transverse anion shifts significantly increase both Mo–X and K(2)–X distances (for a fixed a_p) and hence significantly reduce the over-bonding of the Mo and K(2) ions and also that of the F and O ions (cf., for example, Fig. 3(a) with Fig. 2), although the reduction in AV of the latter ions will be offset to at least some extent by a relatively more minor increase in strength of the anion bonding to neighboring K(1) ions (note that this latter more minor increase has not been taken into account in Fig. 3). The under-bonding of the K(1) ions will also be improved by

such transverse shifts of the anions. The latter is not so clear cut, however, as it will depend upon how the K(1) ions move in response to local distortions of their co-ordination environment caused by the transverse shifts of the anion positions and this is simply not known (the $\Delta(AV)/AV$ curve for K(1) has thus not been included in Fig. 3). These large amplitude, transverse anion shifts could, in principle, be associated either with the additional satellite reflections observed in the room temperature polymorphic form and/or with the observed diffuse distribution [11].

It is worthwhile pointing out at this stage that this proposed transverse anion motion is likely to involve rotation of the MoX_6 octahedra but not necessarily the $K(2)X_6$ octahedra (only the MoX_6 octahedra of the ideal elpasolite structure type are thus shaded in Fig. 1). The ideal Mo–X separation distance of 1.862 Å (assuming O_3F_3 co–ordination) implies an anion–anion separation distance within an MoX_6 octahedra of $1.862\sqrt{2} = 2.633$ Å, close to the minimum possible non-bonded anion–anion separation distance and suggests that the MoX_6 octahedra must move, i.e., rotate or translate, essentially as a rigid unit. The same, however, is not true for the $K(2)X_6$ "octahedra".

A second type of structural distortion (that must be occurring on the local scale simultaneously with the above transverse anion shifts) is needed to reduce the significant difference in the $\Delta(AV)/AV$ curves for O and F apparent in Fig. 2. That this difference cannot be remedied by MoX_6 octahedral rotation alone is apparent from a comparison of Fig. 3(a) (which shows $\Delta(AV)/AV$ curves after transverse anion shifts of 0.75 Å have been taken into account) with Fig. 2. Ideally these two curves should overlap. Given that by far the major contributor to the AV of both O and F ions is the bond they form to their neighboring Mo ion, the only realistic way for the two curves in Figs. 2 and 3(a) to be brought together is for Mo ions to move away from F ions and towards O ions in the local MoX_6 octahedra. This presupposes that opposite vertices in each MoX_6 octahedra are occupied the one by O ions and the other by F ions giving rise to MoO_3F_3 octahedra. Crystal chemical considerations thus suggest that the local co-ordination of each Mo ion should be O_3F_3 with O and F at opposite vertices and with Mo ions moving away from the F's and towards the O's. The magnitude of these induced Mo ion shifts is estimated to be ~0.1 Å from the point of view of obtaining the most reasonable possible local crystal chemistry. (The $\Delta(AV)/AV$ curves in Fig. 3(b), for example, are calculated assuming transverse anion displacements of 0.75 Å combined with Mo ion shifts of 0.105 Å magnitude away the F ions and towards the O ions within each local MoO_3F_3 octahedra. Note the crystal chemical reasonableness of these curves for x ~0.197–0.200).

Crystal chemical considerations thus suggest that both large amplitude, transverse anion shifts associated with MoX_6 octahedral rotation as well as O/F ordering and associated Mo ion shifts are required on the local scale. (Note that the expected larger magnitude of the transverse anion shifts relative to the Mo ion shifts is balanced by the rather larger scattering power of the Mo ions relative to that of the anions so that both types of structural distortion could be expected to have a significant and roughly comparable diffraction effect). Both types of structural distortion could, in principle, be associated either with the additional satellite reflections observed in the room temperature polymorphic form and/or with the observed diffuse distribution [11]. The fact that the satellite reflections disappear suddenly upon heating through the α to β phase transition at ~436 K [5] whereas the diffuse distribution does not [11] suggests to us that the satellite reflections must have a displacive, rather than a diffusion controlled order–disorder, origin. It thus seems much more likely that the observed diffuse distribution arises primarily from O/F ordering and associated Mo shifts than from MoX_6 octahedral rotations (a sudden re-distribution of O/F ordering upon heating through the α to β phase transition at ~436 K seems distinctly unlikely).

Can the observed diffuse distribution provide experimental evidence for such a conclusion?

3. The observed characteristic diffuse distribution

Fig. 4 shows (a) $\langle 3\bar{3}1 \rangle_p$, (b) $\langle 20\bar{1} \rangle_p$, (c) $\langle 1\bar{1}0 \rangle_p$ and (d) $\langle \bar{1}13 \rangle_p$ zone axis electron diffraction patterns (edp's) typical of $K_3MoO_3F_3$. The "sharp", highly structured, essentially continuous nature of the characteristic (and always present) diffuse intensity distribution is immediately apparent. While there is some evidence that the fine details of the shape of the observed diffuse distribution is dependent upon the polymorphic form, the similarity of the diffuse scattering observed at zone axis orientations that would be equivalent in the high temperature cubic $Fm\bar{3}m$ form but become nominally distinct in the monoclinic room temperature $I1a1$ form (cf., for example, Fig. 6(a) and (b) of [11]) shows that this dependence is rather weak. The weak additional satellite reflections present in Fig. 4(b) and (d), for example, have been shown to disappear suddenly upon heating above the polymorphic α to β phase transition. The characteristic diffuse distribution, however, does not and appears to be essentially invariant with respect to both temperature and polymorphic form. (Unfortunately, the sensitivity of the material to electron beam irradiation, particularly at higher temperatures, makes it virtually impossible to undertake a systematic temperature-dependent investigation). As discussed above, this suggests to us that the

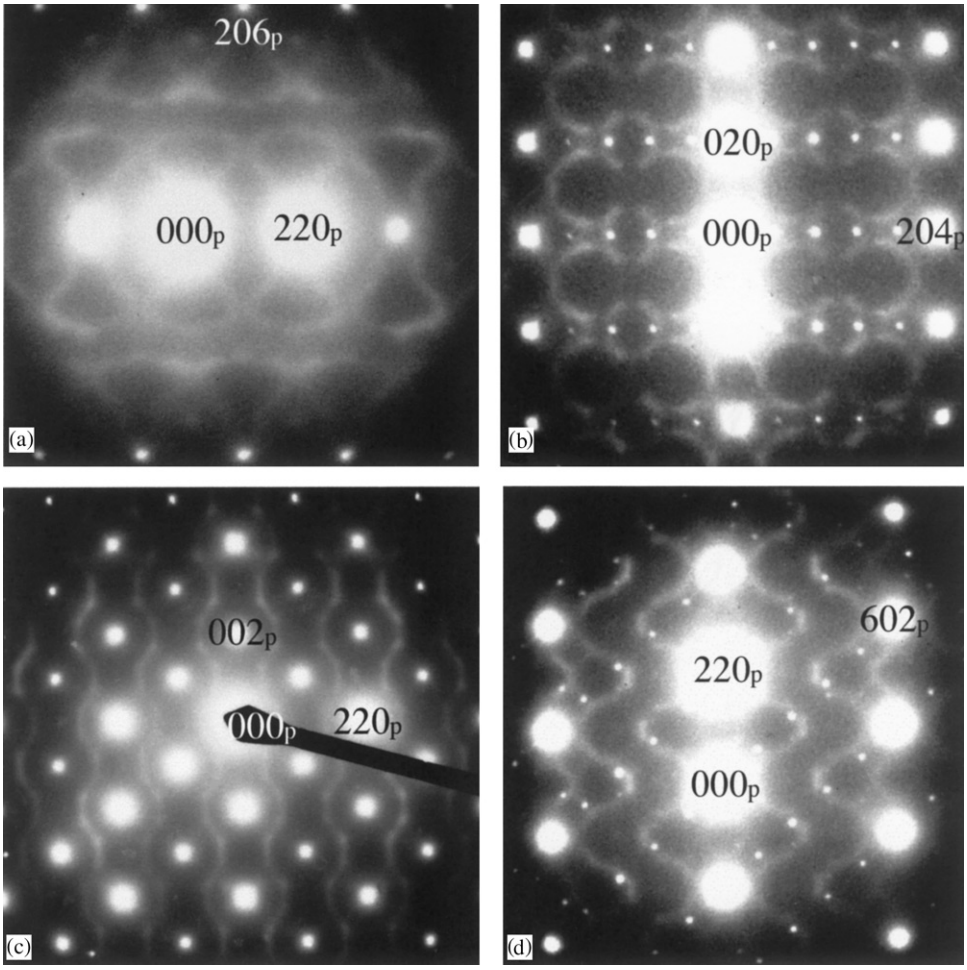

Fig. 4. (a) $\langle 3\bar{3}1\rangle_p$, (b) $\langle 20\bar{1}\rangle_p$, (c) $\langle 1\bar{1}0\rangle_p$ and (d) $\langle \bar{1}13\rangle_p$ zone axis EDP's characteristic of $K_3MoO_3F_3$. Indexation is with respect to the underlying parent structure.

observed diffuse distribution is more likely associated with O/F ordering and associated structural relaxation.

The shape of this observed diffuse distribution is strongly reminiscent of that characteristic of VC_{1-x} and other substoichiometric transition metal carbides and nitrides [17,18]. (The latter phases are of NaCl average structure type with the same average structure space group type as $K_3MoO_3F_3$ i.e., $Fm\bar{3}m$. In the case of VC_{1-x}, Sauvage and Parthé [18] showed that a very good zeroth order approximation to the observed diffuse distribution was given by the equation

$$\cos \pi h + \cos \pi k + \cos \pi l = 0. \quad (1)$$

Calculation of the shape of the diffuse intensity distribution to be expected at each of the zone axis orientations of Fig. 4 shows that Eq. (1) does indeed provide an excellent zeroth order approximation to the observed diffuse intensity distribution in $K_3MoO_3F_3$. The question becomes what is the real space significance of such a diffuse distribution?

4. Theoretical considerations

Sauvage and Parthé [18] used the shape of the observed diffuse distribution in VC_{1-x} and related phases to extract a conventional series of two body Cowley–Warren short range order parameters describing the distribution of vacancies on the "disordered" FCC C sub-lattice. Subsequently de Ridder et al. [19,20], following earlier work of Brunel et al. [21], re-wrote the above expression in exponential form as

$$\begin{aligned}&\exp 2\pi i q\cdot \tfrac{1}{2}\mathbf{a}+\exp 2\pi i\mathbf{q}\cdot -\tfrac{1}{2}\mathbf{a}\\&\quad+\exp 2\pi i\mathbf{q}\cdot \tfrac{1}{2}\mathbf{b}+\exp 2\pi i\mathbf{q}\cdot -\tfrac{1}{2}\mathbf{b}\\&\quad+\exp 2\pi i\mathbf{q}\cdot \tfrac{1}{2}\mathbf{c}+\exp 2\pi i\mathbf{q}\cdot -\tfrac{1}{2}\mathbf{c}=0,\end{aligned}$$

where $\mathbf{q}=h\mathbf{a}^*+k\mathbf{b}^*+l\mathbf{c}^*$ and re-interpreted the significance of Eq. (1) in terms of a six-body octahedral cluster relationship—namely, a requirement that each transition metal ion should always be surrounded by the average number of C or N atoms i.e., there should as far as possible be only one vacancy

in the nearest-neighbor octahedron of available sites (at $\mathbf{T}\pm\frac{1}{2}\mathbf{a}, \mathbf{T}\pm\frac{1}{2}\mathbf{b}$ and $\mathbf{T}\pm\frac{1}{2}\mathbf{c}$, $\mathbf{T}$ a Bravais lattice vector) surrounding each transition metal ion (at $\mathbf{T}$). In the language of composition modulation waves (see Refs. [22,23] for the notation used),

$$\begin{aligned}\delta f(\mathbf{T}+\tfrac{1}{2}\mathbf{a})+\delta f(\mathbf{T}-\tfrac{1}{2}\mathbf{a})+\delta f(\mathbf{T}+\tfrac{1}{2}\mathbf{b})+\delta f(\mathbf{T}-\tfrac{1}{2}\mathbf{b})\\ +\delta f(\mathbf{T}+\tfrac{1}{2}\mathbf{c})+\delta f(\mathbf{T}-\tfrac{1}{2}\mathbf{c})\propto\exp(2\pi i\mathbf{q}\cdot\mathbf{T})\\ \times\{\cos 2\pi\mathbf{q}\cdot\tfrac{1}{2}\mathbf{a}+\cos 2\pi\mathbf{q}\cdot\tfrac{1}{2}\mathbf{b}+\cos 2\pi\mathbf{q}\cdot\tfrac{1}{2}\mathbf{c}\}\\ =\exp(2\pi i\mathbf{q}\cdot\mathbf{T})\{\cos\pi h+\cos\pi k+\cos\pi l\}\end{aligned}$$

should always equal zero regardless of the transition metal ion i.e., regardless of primitive parent unit cell ($\mathbf{T}$). The only modulation wave-vectors $\mathbf{q}$ compatible with this requirement must then satisfy the equation $\cos\pi h+\cos\pi k+\cos\pi l=0$ as required.

In the case of $K_3MoO_3F_3$, the analogous requirement would be that each Mo (or K(2)) ion always be surrounded by the average number of anions i.e., by 3 O's and 3 F's. Such a local O/F ordering constraint would not, however, be sufficient in and of itself to generate the observed diffuse in the current case as the (nominally disordered) anion sites forming an octahedra around each Mo (and K(2) site) are not at $\pm\frac{1}{2}\mathbf{a}$, $\pm\frac{1}{2}\mathbf{b}$, $\pm\frac{1}{2}\mathbf{c}$ with respect to the central cation but rather occur at $\mathbf{r}_{1,2}=\pm x\mathbf{a}$, $\mathbf{r}_{3,4}=\pm x\mathbf{b}$, $\mathbf{r}_{5,6}=\pm x\mathbf{c}$, $x\sim 0.20$, in the case of the Mo ions (and at $\pm(\frac{1}{2}-x)\mathbf{a}$, $\pm(\frac{1}{2}-x)\mathbf{b}$, $\pm(\frac{1}{2}-x)\mathbf{c}$ in the case of the K(2) ions). This does not mean that there is no local O/F ordering within each MoX_6 (or K(2)X_6) octahedra, just that any such ordering is insufficient on its own to produce the observed diffuse distribution. Rather the octahedral cluster relationship giving rise to the observed diffuse scattering can only be associated either with the octahedron of MoX_6 octahedra surrounding each K(2) ion (at $\pm\frac{1}{2}\mathbf{a}$, $\pm\frac{1}{2}\mathbf{b}$, $\pm\frac{1}{2}\mathbf{c}$ with respect to the central K(2) cation; see Fig. 5) or alternatively the octahedron of K(2)X_6 octahedra surrounding each Mo ion. The former seems much more the likely in practice given the difference in oxidation state between the Mo and K ions and the above discussion of local crystal chemical considerations.

Given the similarity in scattering power of oxygen and fluorine for any of the common diffraction techniques [12,13], it is clear that the observed diffuse distribution cannot be directly due to local O/F ordering but rather

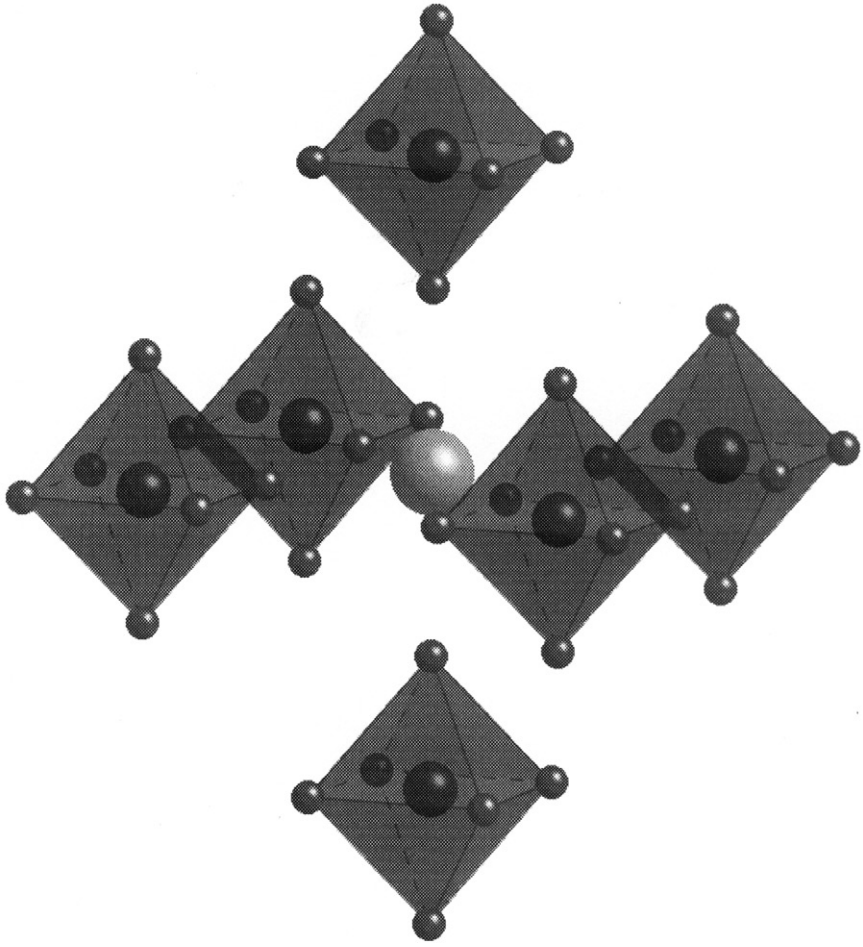

Fig. 5. Octahedra of MoX_6 octahedra surrounding each K(2) cation at $\pm\frac{1}{2}\mathbf{a}$, $\pm\frac{1}{2}\mathbf{b}$ and $\pm\frac{1}{2}\mathbf{c}$.

must primarily be due to cation shifts, most likely Mo cation shifts, associated with O/F ordering. Local crystal chemical considerations (discussed above) support such a conclusion. The same was also true for both of the previously studied cases of FeOF and NbO_2F, where the opposite corners of each local octahedra tended to be occupied one by O and the other by F. In turn, this local O/F ordering pattern induced Fe and Nb shifts away from the F's and towards the O's within each local octahedra [15,16].

It has therefore been assumed in the current case that each Mo ion is always surrounded by 3 O's and 3 F's, that opposite vertices are always occupied the one by O and the other by F and furthermore that the Mo ions initially in the center of each such octahedron will always move away from the F ions and towards the O ions. This leads to the creation of an $(MoO_3F_3)^{3-}$ dipole moment of local $3m$ point group symmetry polarized in either the + or − sense along one of the 4 possible local $\langle 111 \rangle$ real space directions. The direction of the local Mo ion shift defines both the orientation and sense of the local dipole moment. If all these $(MoO_3F_3)^{3-}$ dipole moments were aligned it would obviously lead to a macroscopic spontaneous polarization or dipole moment per unit volume. The constraint upon these Mo ion shifts implied by the observed diffuse distribution (see the appendix for a mathematical derivation) is that

$$\begin{aligned}&\mathbf{u}_{\mathrm{Mo}}(\mathbf{r}_{\mathrm{K2}}+\mathbf{T}+\tfrac{1}{2}\mathbf{a})+\mathbf{u}_{\mathrm{Mo}}(\mathbf{r}_{\mathrm{K2}}+\mathbf{T}-\tfrac{1}{2}\mathbf{a})\\&\quad+\mathbf{u}_{\mathrm{Mo}}(\mathbf{r}_{\mathrm{K2}}+\mathbf{T}+\tfrac{1}{2}\mathbf{b})+\mathbf{u}_{\mathrm{Mo}}(\mathbf{r}_{\mathrm{K2}}+\mathbf{T}-\tfrac{1}{2}\mathbf{b})\\&\quad+\mathbf{u}_{\mathrm{Mo}}(\mathbf{r}_{\mathrm{K2}}+\mathbf{T}+\tfrac{1}{2}\mathbf{c})+\mathbf{u}_{\mathrm{Mo}}(\mathbf{r}_{\mathrm{K2}}+\mathbf{T}-\tfrac{1}{2}\mathbf{c})=0,\end{aligned}\qquad(2)$$

i.e., the Mo shifts in the MoO_3F_3 octahedra surrounding each K(2) ion (see Fig. 5) must always sum to zero. (For a derivation of the relation between Eqs. (1) and (2) in the language of modulation waves see the appendix). Essentially this constraint is equivalent to a requirement that the spontaneous polarization or dipole moment per unit volume (arising from the $(MoO_3F_3)^{3-}$ octahedra) is not only zero macroscopically but also on the unit cell scale.

5. Monte Carlo modelling and simulation results

Monte Carlo simulation was thus used to produce a real space O/F and associated Mo shift distribution that satisfied as far as possible the above constraint. That such a constraint does indeed give rise to a diffuse distribution closely related to that observed experimentally is apparent from simulated diffraction patterns obtained from the resultant real space distribution as shown in Fig. 6. The extraordinary similarity of Fig. 6 to Fig. 4 is immediately apparent.

The MC simulations were carried out as follows. A simulation volume was used which comprised $32\times32\times32$ parent elpasolite type unit cells, each of which included 4 $Mo(O/F)_6$ octahedra. The local conformation of these octahedra was defined in terms of three sets of binary $(-1,+1)$ random variables $u_{i,j,k,l}, v_{i,j,k,l}, w_{i,j,k,l}$, where i,j,k,l are indices defining the parent unit cell along with the particular $Mo(O/F)_6$ octahedra within that unit cell. These binary variables served two purposes. Firstly they were used to define which type of anion (O or F) was the nearest neighbor to the central Mo ion in each of the three mutually orthogonal directions. Secondly, they were used to define a displacement shift from its ideal average position of the Mo cation itself. Thus for example a value of $u_{i,j,k,l}=+1$ for a Mo at (0,0,0) would mean that the anion site at $(x,0,0)$ was occupied by O and that at $(-x,0,0)$ by F. At the same time the Mo itself would be displaced away from the F and towards the O. Conversely for a value of $u_{i,j,k,l}=-1$ the O and F would be interchanged and the Mo displacement would be reversed. Similarly the variables $v_{i,j,k,l}$ and $w_{i,j,k,l}$ corresponded to analogous arrangements of O/F neighbors and the associated Mo displacements in the y- and z-directions, respectively. (In all the calculations the value of x was assumed to be 0.20 and the magnitude of the Mo shift was assumed to be ±0.011 (fractional co-ordinate shifts) $\sim\ \pm0.095$ Å).

The above formulation automatically constrains every $Mo(O/F)_6$ octahedron to contain 3O and 3F. This means that each octahedron is in one of eight different orientations where the triangular face containing 3O's points towards one of the eight $\langle 111 \rangle$ directions, as does the associated Mo displacement vector. (Since $K(2)(O/F)_6$ octahedra occur between these $Mo(O/F)_6$ octahedra and share the same anions, it is interesting to consider how the distribution of O and F in these octahedra is affected by the anion ordering in the Mo octahedra. Table 1 contains some statistics of this distribution before and after the simulation). The quantity minimized in the MC simulation was an energy defined as

$$E_{\mathrm{local}}=\sum K[(\bar{u})^2+(\bar{v})^2+(\bar{w})^2],\qquad(3)$$

where

$$\bar{u}=\sum_1^6 u_{i,j,k,l},\quad \bar{v}=\sum_1^6 v_{i,j,k,l},\quad \bar{w}=\sum_1^6 w_{i,j,k,l}.$$

Here $(\bar{u}),(\bar{v}),(\bar{w})$ are the respective sums of the six $u_{i,j,k,l}, v_{i,j,k,l}, w_{i,j,k,l}$ random variables corresponding to the 6 nearest-neighboring Mo sites that surround a given K(2) site i.e., the energy E_{local} attempts to provide that the net displacement of Mo cations is constrained to zero over the first octahedral shell surrounding any given K(2) ion, as described in Eq. (2) above.

Simulation was carried out for 200 MC cycles, where one cycle is defined as that number of individual MC

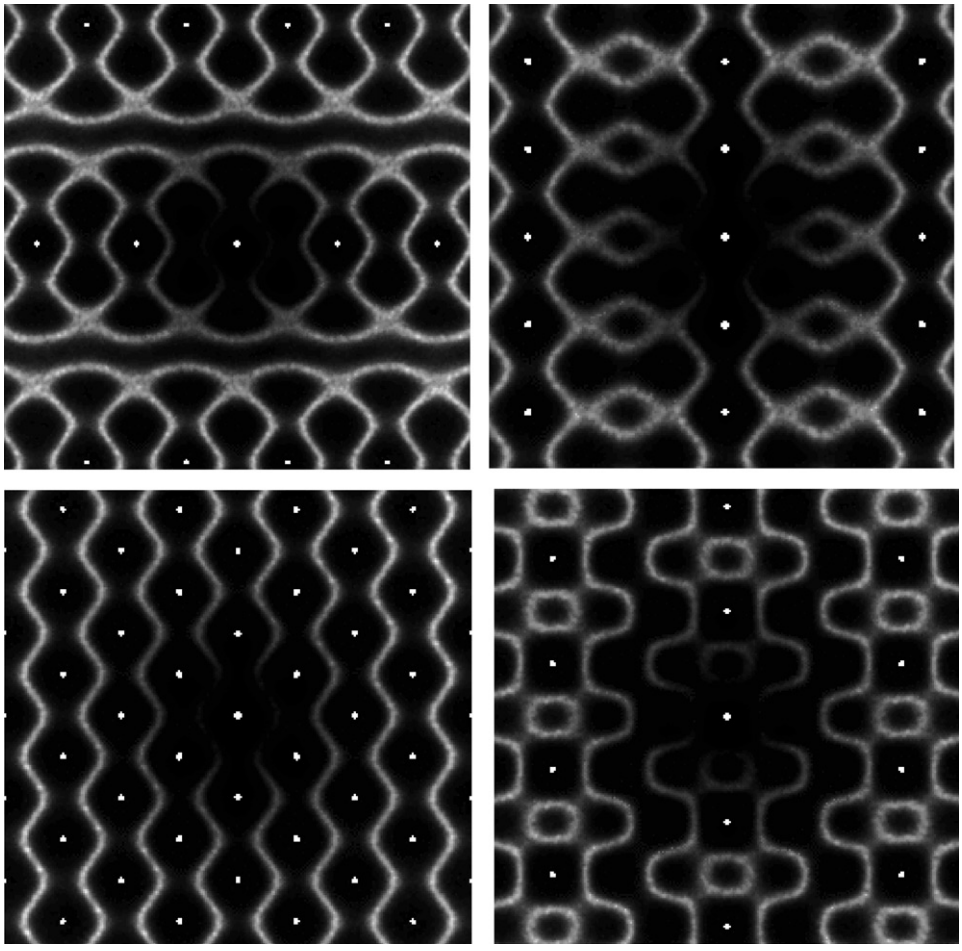

Fig. 6. Simulated (a) $\langle 3\bar{3}1\rangle_p$, (b) $\langle 20\bar{1}\rangle_p$, (c) $\langle 1\bar{1}0\rangle_p$ and (d) $\langle \bar{1}13\rangle_p$ zone axis EDP's for comparison with Fig. 4. Monte Carlo simulation was used to produce a real space O/F and associated Mo shift distribution that satisfied as far as possible the constraint given in Eq. (2). Note the extraordinary similarity of the simulated EDP's in Fig. 6 to the experimentally observed EDP's of Fig. 4.

Table 1

Fractions of the different anion configurations for the K(2) octahedra.							
Configuration	6O	5O + F	4O + 2F	3O + 3F	2O + 4F	O + 5F	6F
Initial random	0.0156	0.0934	0.2342	0.3145	0.2331	0.0929	0.0163
After 200 cycles	0.0221	0.1036	0.2284	0.2915	0.2287	0.1040	0.0217

Mean values of displacement variables for the six Mo atoms around a given K(2)		
Lattice average	$\langle \lvert u_1+u_2+u_3+u_4+u_5+u_6\rvert \rangle$	$\langle \lvert u_1+u_2+u_3+u_4+u_5+u_6\rvert^2 \rangle^{1/2}$
Initial random	1.876	2.449
After 200 cycles	0.447	0.947

steps required to visit each Mo site once on average. Each random variable was initially set to be arbitrarily +1 or –1. At each step in the iteration the random variables at two different *i,j,k,l* sites were interchanged and the effect on the total energy of the system computed. In this way the total numbers of +1 and –1 values was maintained throughout the simulation. As the iteration proceeded various lattice averages were monitored and these are given in Table 1.

Diffraction patterns were calculated from the final distributions using only the Mo positions. These calculations, made with the program DIFFUSE [24], obtained the diffraction pattern by taking the average of a large number of sub-regions (lots) of the main simulation array. In the present case each computed pattern was obtained as an average of 400 individual lots, each of size $10\times10\times10$ unit cells, and utilized ~4 h CPU time on a Pentium III processor.

The figures given in Table 1 demonstrate a number of points. Firstly it is apparent that the ordering of the $Mo(O_3F_3)$ orientations has only a relatively small effect on the frequencies with which different anion arrangements occur in the K(2) octahedra, although the changes that do occur tend to reduce the number of those configurations which have equal numbers of F and O and increase those that are predominantly O or predominantly F. Attempts were made to incorporate an additional term in the Monte Carlo energy which would constrain the distributions of anions in the K(2) octahedra to comprise only (2O + 4F), (3O + 3F) and (4O + 2F) combinations. It proved quite feasible to do this but the resulting effects on the diffuse scattering patterns were quite deleterious.

The second point demonstrated by the figures in Table 1 is that it has not been entirely possible to satisfy for all K(2) sites the rule that the displacements of the 6 Mo atoms that surround any given K(2) octahedron should all sum to zero (see Eq. (2)). Nevertheless the lattice averages in real space (along with the simulated diffraction patterns in reciprocal space) show that substantial progress toward this ideal has been achieved. Increasing the number of cycles further would undoubtedly enable even further progress to be made although ever more slowly and at the expense of increased computational time.

6. Conclusions

The great qualitative similarity of Fig. 6 to Fig. 4 demonstrates that O/F ordering and associated induced Mo ion shifts satisfying the local crystal chemical constraint represented by Eq. (2) are indeed capable of providing an excellent zeroth order explanation for the observed characteristic diffuse intensity distribution. (There are nonetheless differences in fine detail (cf. in fine detail, for example, Fig. 4b with Fig. 6b in the current paper and Fig. 6a with b in [11]) which suggest that the lowering of symmetry from cubic to monoclinic associated with the satellite reflections has also weakly perturbed the shape of the diffuse distribution from the cubic symmetry of Eq. (1) above to a monoclinic shape and therefore somehow needs to be taken into account in order to obtain an even more quantitative fit to the experimental data).

Whether the contribution of O/F ordering and associated induced Mo ion shifts is the only contribution to the observed diffuse distribution, however, is not so clear. On the local scale, both MoO_3F_3 octahedral rotation as well as O/F ordering and induced Mo ion shifts must simultaneously co-exist from the point of view of obtaining satisfactory local crystal chemistry. It is thus possible that the shape (although not necessarily the intensity distribution) of the observed diffuse distribution could equally well be mimicked by a similar constraint to that given in Eq. (2) above, but this time applied to the local pattern of MoO_3F_3 octahedral rotations around each K(2) ion. If, for example, each local MoO_3F_3 octahedra were to rotate in a clockwise sense about the direction of the local induced Mo ion shift, then the local MoO_3F_3 octahedral rotation would be directly tied to the local induced Mo ion shift and would presumably give rise to the same diffuse intensity distribution. Whether this is or is not the case, however, is not possible to quantitatively determine from the data we have to hand.

How the two types of structural distortion simultaneously co-exist in real space thus remains unclear as does the closely related question of whether the resultant diffraction effects are necessarily tied together. It is interesting to note in the case of NbO_2F [16] that the diffuse distribution associated with local O/F ordering (and associated structural relaxation) takes a completely different form to that associated with the octahedral rotation degrees of freedom. This at least provides a precedent for suggesting that the sharp satellite reflections of the room temperature polymorph might well be associated solely with the MoO_3F_3 octahedral rotation and associated K(1) and K(2) displacive degrees of freedom (potentially instantaneously re-orientable upon heating through the α to β phase transition) while the (essentially invariant) diffuse distribution should be attributed to local O/F ordering (and associated Mo shifts) (not instantaneously re-orientable upon heating through the α to β phase transition). Reversible spontaneous polarization at room temperature [7] could then also, at least in principle, be understood without requiring a (highly unlikely) simultaneous re-distribution of O/F ordering. Proof of this contention, however, is far from straightforward and would require either a successful room temperature superstructure refinement (distinctly non-trivial given the unavoidable problems associated with twinning and pseudo-symmetry [11]) and/or extensive further Monte Carlo modelling and simulation as well as more quantitative diffuse data collection, well beyond the scope of the current contribution.

Appendix A

In the language of compositional modulation waves [22,23], the requirement that each Mo ion should always be surrounded by 3O's and 3 F's and that opposite vertices should always be occupied the one by O and the other by F can be ensured by writing

$$\delta f_{1,2}(\mathbf{r}_{1,2}+\mathbf{T}) = \Sigma_{\mathbf{q}} a(\mathbf{q})\cos(2\pi\mathbf{q}.\mathbf{T} + \theta_{12}(\mathbf{q}) \pm 90^\circ),$$
$$\delta f_{3,4}(\mathbf{r}_{3,4}+\mathbf{T}) = \Sigma_{\mathbf{q}} a(\mathbf{q})\cos(2\pi\mathbf{q}.\mathbf{T} + \theta_{34}(\mathbf{q}) \pm 90^\circ),$$
$$\delta f_{5,6}(\mathbf{r}_{5,6}+\mathbf{T}) = \Sigma_{\mathbf{q}} a(\mathbf{q})\cos(2\pi\mathbf{q}.\mathbf{T} + \theta_{56}(\mathbf{q}) \pm 90^\circ).$$

The 180° phase shift between $\delta f_1(\mathbf{r}_1+\mathbf{T})$ and $\delta f_2(\mathbf{r}_2+\mathbf{T})$ etc., for each individual modulation wave–vector $\mathbf{q}$ etc. ensures that opposite vertices are necessarily always occupied the one by O and the other by F. The induced local Mo ion shift along $\mathbf{a}$, $\mathbf{u}_{\mathrm{Mo},x}(\mathbf{T})$ is then proportional to

$$\begin{aligned}&\mathbf{u}_{\mathrm{Mo},x}(\mathbf{T})\alpha\delta f_1(\mathbf{r}_1+\mathbf{T})-\delta f_2(\mathbf{r}_2+\mathbf{T})\\&\quad=2\delta f_1(\mathbf{r}_1+\mathbf{T})\alpha\Sigma_{\mathbf{q}}a(\mathbf{q})\\&\qquad\times\cos(2\pi\mathbf{q}\cdot\mathbf{T}+\theta_{12}(\mathbf{q})+90^\circ).\end{aligned}$$

The x component of Eq. (2) when written in this form (note that $\mathbf{r}_{\mathrm{K}2}+\frac{1}{2}\mathbf{a}\equiv a$ Bravais lattice vector $\mathbf{T}$) is given by

$$\begin{aligned}&\mathbf{u}_{\mathrm{Mo},x}(\mathbf{T})+\mathbf{u}_{\mathrm{Mo},x}(\mathbf{T}+\tfrac{1}{2}[\mathbf{a}-\mathbf{b}])+\mathbf{u}_{\mathrm{Mo},x}(\mathbf{T}+\tfrac{1}{2}[\mathbf{a}+\mathbf{b}])\\&\quad+\mathbf{u}_{\mathrm{Mo},x}(\mathbf{T}+\mathbf{a})+\mathbf{u}_{\mathrm{Mo},x}(\mathbf{T}+\tfrac{1}{2}[\mathbf{a}-\mathbf{c}])\\&\quad+\mathbf{u}_{\mathrm{Mo},x}(\mathbf{T}+\tfrac{1}{2}[\mathbf{a}+\mathbf{c}])=0\end{aligned}$$

and is thus directly proportional to

$$\begin{aligned}&\Sigma_{\mathbf{q}}\{\cos(2\pi\mathbf{q}\cdot\mathbf{T}+\theta_{12}+90^\circ+\pi h-\pi h)\\&\quad+\cos(2\pi\mathbf{q}\cdot\mathbf{T}+\theta_{12}+90^\circ+\pi h-\pi k)\\&\quad+\cos(2\pi\mathbf{q}\cdot\mathbf{T}+\theta_{12}+90^\circ+\pi h+\pi k)\\&\quad+\cos(2\pi\mathbf{q}\cdot\mathbf{T}+\theta_{12}+90^\circ+\pi h+\pi h)\\&\quad+\cos(2\pi\mathbf{q}\cdot\mathbf{T}+\theta_{12}+90^\circ+\pi h-\pi l)\\&\quad+\cos(2\pi\mathbf{q}\cdot\mathbf{T}+\theta_{12}+90^\circ+\pi h+\pi l)\}\\&=\Sigma_{\mathbf{q}}\cos(2\pi\mathbf{q}\cdot\mathbf{T}+\theta_{12}+90^\circ+\pi h)\\&\quad\times\{\cos\pi h+\cos\pi k+\cos\pi l\}.\end{aligned}$$

The requirement that this should always equal zero regardless of $\mathbf{T}$ can thus only be satisfied if individual modulation wave–vectors $\mathbf{q}=h\mathbf{a}^*+k\mathbf{b}^*+l\mathbf{c}^*$ satisfy the constraint equation $\{\cos\pi h+\cos\pi k+\cos\pi l\}=0$ as required.

References

[1] G. Pausewang, P. Rüdorff, Z. Anorg. Allg. Chem. 364 (1969) 69.
[2] J. Ravez, J. Phys. III France 7 (1997) 1129.
[3] G. Meyer, Prog. Solid State Chem. 14 (1982) 141.
[4] I.N. Flerov, M.V. Gorev, K.S. Alexandrov, A. Tressaud, J. Grannec, M. Couzi, Mater. Sci. Eng. Rep. 24 (1998) 81.
[5] G. Péradeau, J. Ravez, P. Hagenmuller, H. Arend, Solid State Commun. 27 (1978) 591.
[6] J. Ravez, G. Péradeau, H. Arend, S.C. Abrahams, P. Hagenmuller, Ferroelectrics 26 (1980) 767.
[7] Z.G. Ye, J. Ravez, J-P. Rivera, J-P. Chaminade, H. Schmid, Ferroelectrics 124 (1991) 281.
[8] P. Hagenmuller, in: K.J. Rao (Ed.), Perspectives in Solid State Chemistry, Narosa, New Delhi, 1995, pp. 66–78.
[9] S.C. Abrahams, J.L. Bernstein, J. Ravez, Acta Crystallogr. B 37 (1981) 1332.
[10] N.E. Brese, M. O'Keeffe, Acta Crystallogr. B 47 (1991) 192.
[11] F.J. Brink, R.L. Withers, K. Friese, G. Madariaga, L. Norén, J. Solid State Chem. 163 (2002) 267.
[12] L. Du, F. Wang, C.P. Grey, J. Solid State Chem. 140 (1998) 285–294.
[13] R.L. Needs, M.T. Weller, J. Chem. Soc. Dalton Trans. (1995) 3015–3017.
[14] T. Vogt, P.M. Woodward, B.A. Hunter, A.K. Prodjosantoso, B.J. Kennedy, J. Solid State Chem. 144 (1999) 228–231.
[15] F.J. Brink, R.L. Withers, J.G. Thompson, J. Solid State Chem. 155 (2000) 359–365.
[16] F.J. Brink, R.L. Withers, J.G. Thompson, J. Solid State Chem. 166 (2002) 73–80.
[17] J. Billingham, P.S. Bell, M.H. Lewis, Acta Crystallogr. A 28 (1972) 602.
[18] M. Sauvage, E. Parthé, Acta Crystallogr. A 28 (1972) 607.
[19] R. de Ridder, G. van Tendeloo, D. van Dyck, S. Amelinckx, Phys. Stat. Sol. (a) 38 (1976) 663.
[20] R. de Ridder, D. van Dyck, G. van Tendeloo, S. Amelinckx, Phys. Stat. Sol. (a) 40 (1977) 669.
[21] M. Brunel, F. de Bergevin, M. Gontrand, J. Phys. Chem. Solids 33 (1972) 1927.
[22] R.L. Withers, S. Schmid, L. Norén, Y. Tabira, J.G. Thompson, Ferroelectrics 250 (2001) 47.
[23] R.L. Withers, S. Schmid, J.G. Thompson, Prog. Solid State. Chem. 26 (1998) 1–96.
[24] B.D. Butler, T.R. Welberry, J. Appl. Crystallogr. 25 (1992) 391–399.